Materials Chemistry

Cite this: *J. Mater. Chem.*, 2011, **21**, 7263

www.rsc.org/materials

PAPER

Intense and wavelength-tunable photoluminescence from surface functionalized MgO nanocrystal clusters†

Shuifen Xie, Xiguang Han, Qin Kuang,* Yang Zhao, Zhaoxiong Xie* and Lansun Zheng

Received 19th February 2011, Accepted 25th March 2011
DOI: 10.1039/c1jm10745c

We report fancy brilliant photoluminescence (PL) from surface functionalized MgO nanocrystal clusters (NCs). Single-crystal-like MgO NCs were prepared by a simple one-pot pyrolysis method in the mixed organic solvent of octylamine (OTA) and oleic acid (OA) using magnesium acetate as a precursor. Under the chemical equilibrium of etching and re-growth with the assistance of OA, the MgO products were surface functionalized. It was found that such surface functionalized MgO NCs exhibited intense visible light PL with high PL thermal-stability, and the apparent quantum yield was as high as 19 ± 1%. In addition, through controlling the synthetic temperature and the reaction time, the functionalized surfaces of MgO NCs were facilely tuned, resulting in the tuneable wavelength of the PL from blue-violet to yellow. Different low-coordinated oxygen sites, capping OA and carbonate species on the surface of the MgO nanocrystals were thought to be the origin of PL at different wavelengths. Considering the intense PL, high PL stability at ambient conditions, low cost and low toxicity, such MgO NCs might have potential applications in medicine and biology as a new kind of fluorescent label.

Introduction

The surface states of inorganic nano-materials have been proved to extensively influence their physical and chemical properties, due to the extremely large surface area and great proportion of low-coordinated surface atoms.[1–3] For this reason, some strategies have been developed to construct specific surface states, such as particular exposed facets,[4–8] ligand-modified surfaces,[9,10] and defective surfaces.[11–13] With these functional surface states, not only can the substantial performance of nano-materials be extremely enhanced, but also sometimes unexpected properties can be enhanced. For example, weak fingerprint photoluminescence (PL) in the UV-visible range was discovered on well-outgassed magnesium oxide (MgO) nano-powders although MgO is a wide-band-gap insulator (7.8 eV).[14–19] Such UV-visible luminescence was assigned to the charge transfer on the surface states, especially depending on the low coordination oxygen ions ($O^{2-}{}_{LC}$).[20–22] And this feature was further developed as a technique to determine the surface $O^{2-}{}_{LC}$ of alkaline earth metal oxides.[15,16] However, the direct optical utilization of the PL properties of MgO is greatly restricted by its weak intensity and the PL quenching in ambient conditions.

Very recently, extensive efforts, such as surface doping,[23–25] size control,[17] and organic ligand modification,[26] have been introduced to further investigate the optical properties of MgO. However, conventional preparation methods based on chemical vapor deposition (CVD) or calcination are not effective enough for controlling the surface states of MgO nanocrystals. For this reason, intense and wavelength-tunable PL emissions of MgO nanocrystals have not been achieved to date. Herein, we report a simple one-pot pyrolysis method to prepare single-crystal-like MgO nanocrystal clusters (NCs) in the mixed organic solvent of octylamine (OTA) and oleic acid (OA) using magnesium acetate as a precursor. Through controlling the synthetic temperature and the heating time, the surface states of MgO nanocrystals were facilely tuned due to the surface etching effect by OA and the functionalization of carboxyl and carbonate on the MgO nanocrystal surfaces. Excitingly, the as-prepared MgO NCs exhibited widely tunable PL emissions from blue-violet to yellow with high quantum yield and high PL thermal-stability. The tuneable PL emissions were attributed to the different low-coordinated sites, capping OA and carbonate species on the surface of the MgO nanocrystals, which were confirmed by UV-visible diffuse reflectance spectroscopy (DRS), electron spin resonance (ESR) techniques and Fourier transform infrared spectroscopy (FTIR).

State Key Laboratory for Physical Chemistry of Solid Surfaces and Department of Chemistry, College of Chemistry and Chemical Engineering, Xiamen University, Xiamen, 361005, P.R. China. E-mail: zxxie@xmu.edu.cn; qkuang@xmu.edu.cn; Fax: +86-592-2183047; Tel: +86-592-2180627

† Electronic supplementary information (ESI) available: N_2 adsorption–desorption isotherms and pore-size distribution curve of MgO400, XRD and SEM of the samples, the thermogravimetric analysis of MgO480, the FTIR spectra of MgO480 samples calcined at different temperatures, the PL spectra of MgO480 before and after calcination, the PL comparison of commercial MgO before and after refluxing at 400 °C. See DOI: 10.1039/c1jm10745c

Experimental

Materials

Magnesium acetate ($Mg(CH_3COO)_2 \cdot 4H_2O$, 99.0%), n-octylamine (OTA, 99%), and oleic acid (OA, 90%) were used in our experiments. All the chemicals were purchased from commercial suppliers (Alfa Aesar). $Mg(CH_3COO)_2 \cdot 4H_2O$ was dehydrated at 135 °C for 10 h before reactions.

Synthesis of luminescent MgO nanocrystal clusters

Anhydrous $Mg(CH_3COO)_2$ (0.710 g, 5.0 mmol), OTA (1.5 mL) and OA (3.5 mL) were added into a long quartz test tube (about 40 cm in length and 2.0 cm in diameter). Then, the bottom of the tube was set on a thermocouple that was in the middle of an erect tubular furnace. Under the control of a program temperature controller, the tubular furnace was heated rapidly to the required temperature within 20 min and kept for 60 min at the temperature. After reactions, the products were cooled naturally to the ambient room-temperature and washed with hexane 5 times with ultrasonic treatment and centrifugation (10000 rpm, 6 min). The products were dried at 60 °C. For further PL characterization, the MgO NCs were dispersed in ethanol solution, and they can be kept for months without apparent aggregation.

Characterization and measurements

The powder X-ray diffraction (XRD) pattern was recorded using a Panalytical X-pert diffractometer with copper Kα irradiation. Scanning electron microscopy (SEM, Hitachi S-4800) and transmission electron microscopy (TEM, JEM 2100, 200 kV) were employed to investigate the morphology and structure of the as-prepared samples. The surface area of the final products was measured by the Brunauer–Emmett–Teller (BET) method using nitrogen adsorption and desorption isotherms on a Micrometrics ASAP 2020 system. The pore size distribution plot was obtained by the Barrett–Joyner–Halenda (BJH) method. UV-visible diffuse reflectance spectroscopy (DRS) was carried out with a Varian Cary-5000 UV-Vis-NIR Spectrophotometer. PL spectra were recorded on a Hitachi F-7000, and the absolute quantum yields were measured on a Jobin Yvon Horiba Fluoromax-4 with an integration sphere. Room-temperature ESR spectra were collected on a Bruker EMX-10/12 Electron Spin Resonance Spectrometer. The Fourier transform infrared spectroscopy (FTIR) was recorded on a Nicolet 330 spectrometer. The thermogravimetric analysis (TGA) was carried out on an SDT Q600 thermal analyzer under an air atmosphere in the temperature range of 30∼1000 °C with a heating rate of 10 °C min^{-1}.

Results and discussion

The MgO NCs were synthesized at a series of temperatures from 320 °C to 480 °C and the products prepared at 320 °C, 360 °C, 400 °C, 440 °C and 480 °C were denoted as MgO320, MgO360, MgO400, MgO440 and MgO480, respectively. As an example, the XRD pattern of MgO400 is shown in Fig. 1a, which demonstrates the successful preparation of pure MgO with a rock-salt structure (JCPDS 43-1022). The corresponding

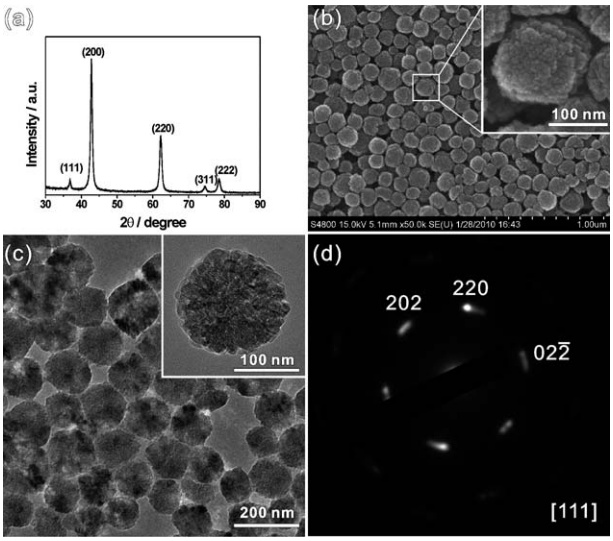

Fig. 1 Composition and morphology of MgO400: (a) XRD pattern, (b) SEM image, (c) TEM image, (d) SAED pattern of an individual MgO NC. Insets in (b) and (c) are magnified images of single MgO NC.

electron microscopic observation (Fig. 1b and c) shows that the sample consists of well-dispersed spherical nanostructures with a uniform diameter of 150 nm, which are built up by numerous MgO nano-grains. The average crystallite size of the nano-grains is calculated to be 19.3 nm by the Scherrer formula depending on the (220) and (200) diffraction peaks, respectively (Table 1). Interestingly, the relevant SAED pattern (Fig. 1d) presents a single-crystal-like feature, indicating these nano-grains in the MgO NCs are well oriented. In addition, the nitrogen adsorption and desorption isotherms reveal that such MgO NCs possess a large BET surface area (91 m^2 g^{-1}) and porosity with small mesopores around 2 nm (Fig. S1†). It should be pointed out that all the other products prepared at different temperatures have the same crystal structure and similar morphology as MgO400 (Fig. S2 and S3†). However, the sizes of nano-grains in the MgO NCs gently decrease from about 27.6 nm to 14.6 nm with the increase in reaction temperature as the width of diffraction peaks broaden with the increase in the reaction temperature (Table 1 and Fig. S2†).

Attractively, the MgO NCs exhibit bright and tunable PL properties. From the PL spectra excited at 325 nm (Fig. 2a), wide emissions are observed in all the MgO NCs, and the emissions markedly red-shift for the products of higher reaction temperature. Fig. 2b–f are the respective PL spectra fitted with the nonlinear least-squares fit program using Gauss-Lorentzian peak shapes. It is clearly found that all the PL emission of each MgO NCs sample consist of three main peaks centred at about 405 nm, 470 nm, and 540 nm although the relative intensities of the three emissions are different with the reaction temperature. For the MgO320, the spectrum is dominated by the purple emission around 405 nm. And for the MgO360, the blue emission at around 470 nm occupies as much portion as the purple emission. When the reaction temperature increases to 400 °C, the emissions around 470 nm and 530 nm become dominant, accompanying the decrease in the ratio of emission around 405 nm. When the reaction temperature further increases, the green emission of

Table 1 Nano-grain size and PL apparent quantum yield of the MgO NCs prepared at different temperatures

Sample No.	MgO320	MgO360	MgO400	MgO440	MgO480
T/°C	320	360	400	440	480
Grain size (d_{220})/nm	24.3	18.5	17.6	14.8	13.6
Grain size (d_{200})/nm	30.9	22.4	20.9	16.8	15.5
Average grain size/nm	27.6	20.5	19.3	15.8	14.6
Quantum yield/%	17 ± 1	19 ± 1	17 ± 1	11 ± 1	7 ± 1

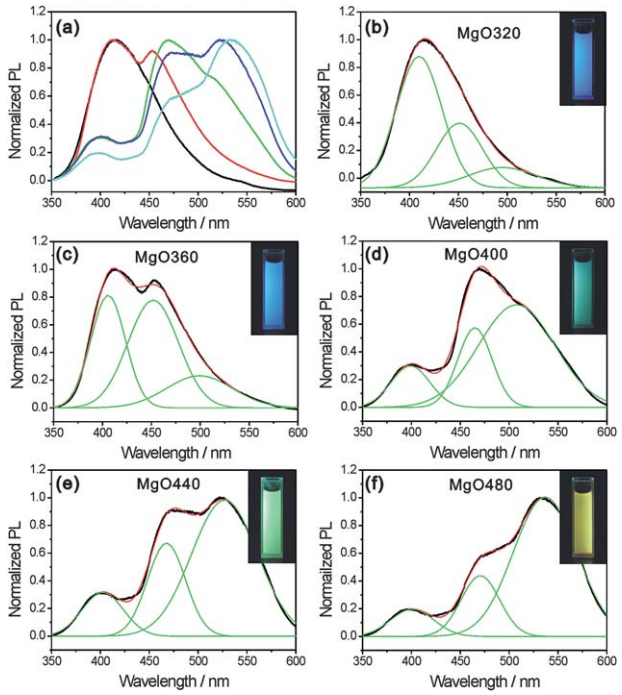

Fig. 2 (a) Room-temperature PL spectra under irradiation at 325 nm of the MgO NCs: MgO320 (black), MgO360 (red), MgO400 (green), MgO440 (blue), MgO480 (cyan). (b)–(f) Respective PL spectra of MgO NCs samples fitted with the nonlinear least-squares fit program using Gauss-Lorentzian peak shapes, and the insets are corresponding optical images under 365 nm irradiation in ethanol.

around 530 nm slightly shifts to 540 nm and its intensity increases, while the intensities of emissions centred at 405 nm and 470 nm decrease. For the MgO480, the primary emission is dominated by the yellow emission around 540 nm. Such wavelength and intensity tunable luminescence, which is even visible by the naked eye, results in the remarkable changes of apparent color (from blue-violet to blue, green and yellow) under the UV light illumination (insets of Fig. 2b–f). It should be in particular pointed out that the MgO NCs synthesized below 400 °C exhibit a high PL apparent quantum yield (QY) (up to 17–19%) under the excitation of 365 nm, and therein the MgO360 possesses the maximal value (19 ± 1)% (Table 1). In comparison with previous studies, the QY value of these MgO NCs is comparative to the data (15–19%) of monodisperse colloidal MgO nanocrystals.[26] For the MgO NCs synthesized over 400 °C, however, the apparent QY value evidently decreases with the increase in synthetic temperature, which is only 7% for MgO480. The QY change might be ascribed to the difference between the types of surface defects, according to the previous study reported by Sternig.[25] Moreover, the PL of the MgO NCs is insensitive to the ambient temperature fluctuation, for the intensity still maintains over 90% when the ambient temperature increases from 30 °C to 65 °C (Fig. 3). And no obvious PL change was observed for these MgO NC powders exposed in the air over several months, indicating that the PL of the MgO NCs is also insensitive to O_2. This is a big advantage for practical application of the MgO NCs, such as fluorescence imaging in fluctuating ambient circumstances.

As a wide-band-gap insulator, MgO usually would not exhibit PL in the visible light region. However, it has been found that charge transfer on the surface states could result in UV-visible luminescence,[20–22] although the surfaces states (that are usually attributed to specific low-coordinated sites) are still ambiguous. For the present case, the MgO grains are on the nanometre scale, which inevitably results in large amounts of surface states. Structurally, MgO belongs to the rock salt structure where Mg^{2+} and O^{2-} ions are both six-coordinated in its bulk. On the rough surface, however, the coordination number of both cations and anions should decrease, which should generate various low-coordinated oxygen sites. According to previous studies,[16,22] both the emissions centred at 405 nm and 470 nm are relevant to pristine and modified three-/four- coordinated (3C/4C) oxygen sites, respectively. The UV-visible DRS measurements (Fig. 4a) support the presence of pristine and modified 3C/4C oxygen sites in our as-prepared MgO NCs. We can find three main shoulder-like absorption features around 270 nm, 365 nm and 440 nm. Costentin and co-workers assigned the optical absorption band at 270 nm to 3C oxygen sites, and 360 nm to protonated and

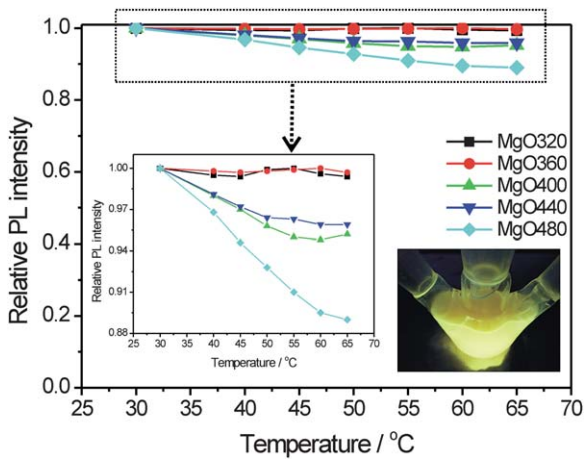

Fig. 3 Relative PL intensity of as-synthesized MgO NCs in ethanol solution from 30 °C to 65 °C showing the thermal stability (bottom right: the optical picture of MgO480 in ethanol heated to 65 °C under 365 nm).

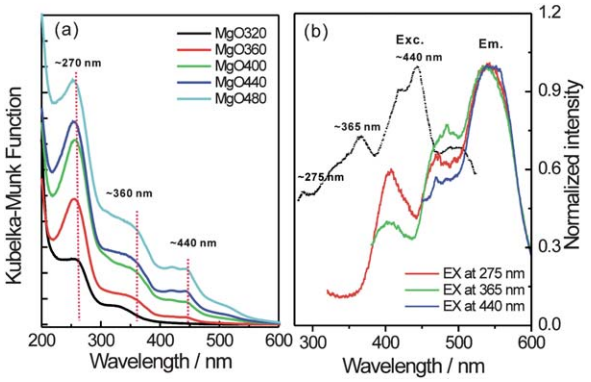

Fig. 4 (a) The room-temperature UV-Vis DRS of MgO NCs samples. (b) The room-temperature excitation spectrum (λ_{em} = 540 nm) and PL emission spectra under 275 nm, 365 nm and 440 nm irradiation of MgO480, respectively.

methylated 3C or 4C oxygen sites.[16] In our case the adsorption at 360 nm could be the protonated or ligand modified ones (such as carboxylated ones) according to our reaction conditions. As for the origin of the adsorption around 440 nm, it will be discussed in the following part of this paper.

To further confirm the origin of the PL emissions, elaborate measurements of the excitation and relevant PL emission spectra were carried out. Fig. 4b shows a representative example of MgO480. The room-temperature excitation spectrum (λ_{em} = 540 nm) in the scanning range from 260 nm to 520 nm shows three relatively obvious excitation centres located around 275 nm, 365 nm and 440 nm, respectively, which are unambiguously correlated to the three adsorptions peaks in the UV-visible measurements. Carefully analyzing the PL spectra respectively excited by the 275 nm, 365 nm and 440 nm irradiations (Fig. 4b, normalized by using the intensity around 540 nm), we may find that the three emissions (centred at about 405 nm, 470 nm, and 540 nm) can be obtained at both 275 nm and 365 nm irradiations, and the 440 nm irradiation mainly results in a strong emission around 540 nm. However, the emission peak around 405 nm is stronger under the 275 nm irradiation than that under the 365 nm irradiation; and on the contrary, the emission around 470 nm is more intense under the 365 nm irradiation than that under the 275 nm irradiation. These results indicate the emission peak around 405 nm is related to the 275 nm irradiation, and the emission around 470 nm to the 365 nm irradiation. Such spectroscopic results are in good agreement with the origins of PL and UV-visible adsorptions reported in the literature.[16] As for the emission around 540 nm, it could be mainly related to the surface states with adsorption at about 440 nm, because the emission around 540 nm is relatively strong under the 440 nm irradiation. It should be pointed out that, due to the energy overlap of the surface states, great self-absorption and self-excitation should occur during the PL process.

However, the origin of the third emission (λ_{em} = 540 nm) and the adsorption at 440 nm were not reported formerly. Oliver Diwald and co-workers have confirmed that the optical properties of MgO should not be regarded as merely a signature of low-coordinated oxygen ions but ought to be assigned to multi-atomic topological features.[21] Because these MgO NCs were synthesized in organic solution and have a rough surface, we believe that they are modified with some ligands at low coordinated sites. To gain further deep insight into the origin of the third emission (540 nm), FTIR spectroscopy and ESR were applied to discern the surface functional groups. The FTIR spectra of the as-prepared MgO NCs (Fig. 5) show a strong adsorption around 520 cm^{-1}, which is due to characteristic stretching of the Mg–O bond in MgO crystals. The broad adsorption bands around 3400 cm^{-1} correspond to the adsorbed water. In addition, the adsorption bands of C–H stretching at 2925 and 2855 cm^{-1} can be distinctly observed in all the MgO NCs, and the two broad absorption bands at 1580 cm^{-1} and 1426 cm^{-1}, corresponding to asymmetric and symmetric COO^- stretching vibrations respectively, are also found. However, the specific bands at 1711 cm^{-1} of C=O in carboxylic acid and 1614 cm^{-1} of N–H in alkylamine are not observed. We therefore conclude that the nanocrystal surface of MgO NCs must be capped with abundant carboxylic groups that come from the mixed organic solution such as OA or acetates. Interestingly, in our MgO NCs, an absorption at 1384 cm^{-1}, which has been assigned to the surface carbonates stretching vibrations on MgO nanopowders,[27] is gradually enhanced with the increase in the reaction temperature. Such surface modification of MgO NCs can be further confirmed by the thermogravimetric analysis that gives a weight loss total of 11.5% in the temperature range from 100 to 800 °C (Fig. S4†) for the MgO480. According to the FTIR spectra (Fig. S5†) of the MgO480 calcined at different temperatures, the weight loss of the MgO NCs should be attributed to the removal of OA capping on the surface of MgO NCs as the adsorption bands assigned to C–H and COO^- stretching vibrations gradually decreased and even disappeared, with the increase in the calcination temperature of MgO NCs. Furthermore, the ESR technique was introduced to determine the configuration of the surface carbonates. Correspondingly, the spectra of as-prepared MgO NCs exhibit a broad ESR resonance with a g tensor of 2.003 (Fig. 6), which is close to that of a free single electron (g = 2.0023). It was proposed that the presence of carbonate on the defect-rich surface of metal oxide could generate a CO_3^- paramagnetic centre, which is planar with D_{3h}

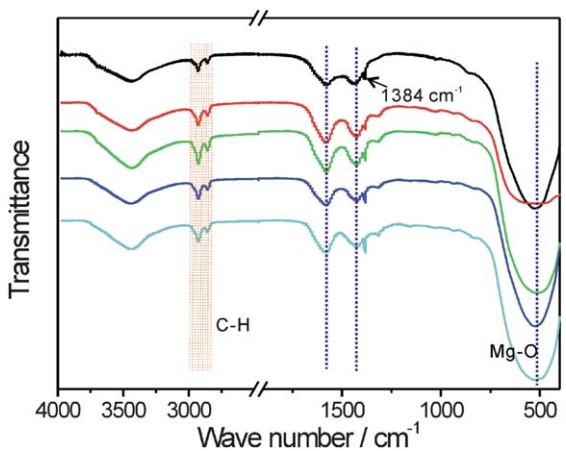

Fig. 5 Room-temperature FTIR spectra of the as-synthesized MgO NCs: MgO320 (black), MgO360 (red), MgO400 (green), MgO440 (blue), and MgO480 (cyan).

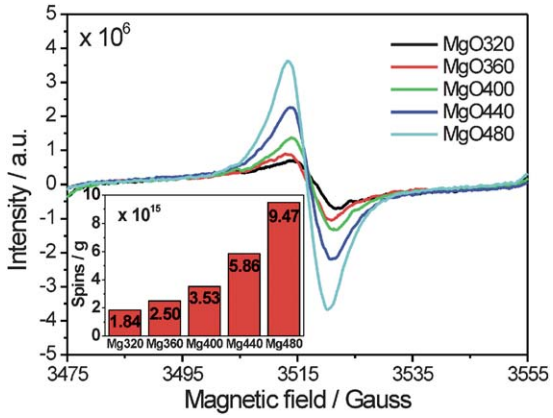

Fig. 6 (a) Room-temperature ESR spectra of the paramagnetic centre from the carbonated low-coordinated surface sites of the as-synthesized MgO NCs; the inset is the corresponding relative spin number using emery rock as standard.

symmetry.[28] Its singly occupied molecular orbital is nonbonding, built up by the out-of-phase combination of in-plane p orbitals of the three oxygen atoms.[28] Such a planar CO_3^- radical can be thought as an s radical with orbital angular momentum $L = 0$, and therefore exhibits free-single-electron-like ESR signal. In addition, the corresponding relative spin number is continuously increased with the increase in the synthetic temperature, indicating the increase in the amount of the modified carbonate site. Such ESR results are in good agreement with the FTIR measurements. Considering the fact of the adsorption around 440 nm, and the intensity of the 540 nm emission increases with reaction temperature, we conclude that the relevant optical absorption at 440 nm and emission at 540 nm species associates to these capped paramagnetic carbonate sites.

The fact that the emissions around 470 nm and 540 nm are originated from surface modifications of OA and carbonate species on the surface of MgO nanocrystals can be proved by annealing the samples at high temperature (Fig. S6†). When annealing the samples at 400 °C, the PL of the MgO NCs shifted to the blue range, and the emissions around 470 nm and 540 nm markedly decreased. When annealing the samples at 800 °C, however, all the emissions disappeared. Obviously, the PL change of MgO NCs should originate from desorption of adsorbed OA and the decomposition of surface CO_3^- paramagnetic centres under high temperature. This conclusion also agrees well with the evidence provided by the TGA analysis (Fig. S4†) and the FTIR spectra (Fig. S5†) of MgO480 calcined at different temperatures.

Our previous works have shown that the OA can simultaneously act as an etchant during the growth of some metal oxide nanocrystals,[29,30] which inevitably creates abundant defective sites, including low-coordinated surface sites, on the surface of nanocrystals. Hence, in this case, the MgO NCs have an abundance of pristine and modified low-coordinated surface sites, leading to the visible light emissions. Obviously, higher reaction temperature is beneficial to the etching of Mg^{2+} on the surface of MgO nanocrystals, resulting in smaller (proved by XRD, Table 1 and Fig. S2†) and rougher grains, and at the same time it is beneficial to the formation of ligand/carbonate-modified lower coordinated oxygen ions. Of course, besides reaction temperature, reaction time is another synthetic parameter to change etching degrees of MgO NCs. Therefore, prolonging the reaction time is thought to play a similar role on tuning the PL properties of MgO NCs with increasing reaction temperature. As evidence, Fig. 7 shows that in either UV-vis adsorption spectra or PL spectra, the change trends are similar to the case of increasing reaction temperature (Fig. 2 and Fig. 4). As shown in Fig. 7c, a prospective PL shift from blue-violet to green-yellow was observed when the reaction time was prolonged from 10 min to 120 min at 400 °C.

It should be pointed out that the UV-visible PL emissions of our MgO NCs depend mainly on the surface defects rather than defects in the bulk. Such a hypothesis can be demonstrated by directly cooking the commercial MgO powder in the solvent of OA and OTA at the same temperature, by which similar PL emissions can be observed (Fig. S7†).

Conclusions

In conclusion, single-crystal-like MgO NCs with intense, wavelength tunable and thermally stable PL from the blue-violet to the yellow were successfully fabricated *via* a one-step pyrolysis route. We prove the tunable PL of as-prepared MgO NCs is achieved under the synergy effects of different surface states, in which PL emissions centred at 405 nm, 470 nm are relevant to pristine and modified three-/four- coordinated (3C/4C) oxygen sites respectively, and that at 540 nm is related to capped CO_3^- paramagnetic centres. Considering the high PL stability at

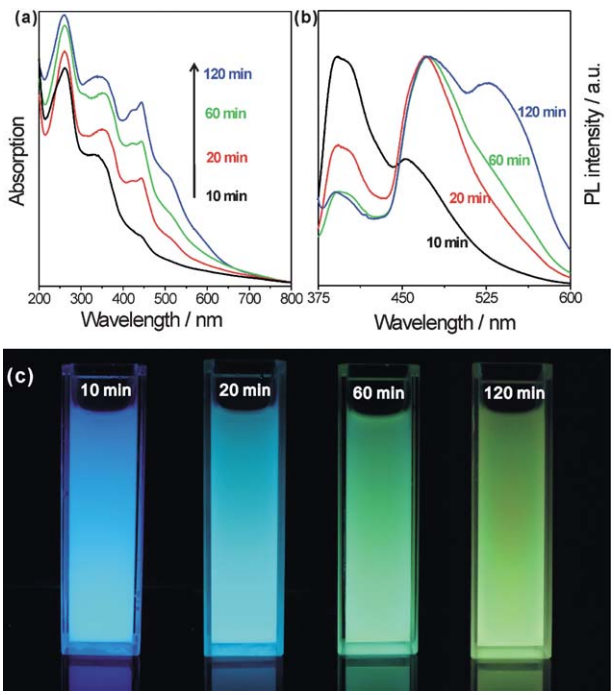

Fig. 7 (a) Room-temperature UV-vis diffuse reflectance spectra, (b) room-temperature PL spectra under irradiation at 365 nm of the MgO NCs obtained at 400 °C with 1.5 mL OTA and 3.5 mL OA for different times (10 min, 20 min, 60 min and 120 min respectively), and (c) corresponding optical image of MgO samples dispersed in ethanol under excitation at 365 nm in a dark-room.

ambient conditions, good biocompatibility, low cost and low toxicity, such MgO NCs might have potential applications in medicine and biology as a new kind of fluorescent label. This strategy represents a promising platform for designing functional nano-materials and exploits feasible optical application of alkaline earth metal oxides.

Acknowledgements

This work was supported by the National Natural Science Foundation of China (Grants 20725310, 20721001, 21073145 and 20801045) and the National Basic Research Program of China (Grants 2007CB815303, 2011CBA00508).

Notes and references

1 R. Narayanan and M. A. El-Sayed, *Nano Lett.*, 2004, **4**, 1343.
2 M. Batzill and U. Diebold, *Prog. Surf. Sci.*, 2005, **79**, 47.
3 G. A. Somorjai, *Prog. Surf. Sci.*, 1995, **50**, 3.
4 X. W. Xie, Y. Li, Z. Q. Liu, M. Haruta and W. J. Shen, *Nature*, 2009, **458**, 746.
5 N. Tian, Z. Y. Zhou, S. G. Sun, Y. Ding and Z. L. Wang, *Science*, 2007, **316**, 732.
6 H. G. Yang, C. H. Sun, S. Z. Qiao, J. Zou, G. Liu, S. C. Smith, H. M. Cheng and G. Q. Lu, *Nature*, 2008, **453**, 638.
7 X. G. Han, Q. Kuang, M. S. Jin, Z. X. Xie and L. S. Zheng, *J. Am. Chem. Soc.*, 2009, **131**, 3152.
8 Y. Y. Ma, Q. Kuang, Z. Y. Jiang, Z. X. Xie, R. B. Huang and L. S. Zheng, *Angew. Chem., Int. Ed.*, 2008, **46**, 8901.
9 S. Banerjee, T. Hemraj-Benny and S. S. Wong, *Adv. Mater.*, 2005, **17**, 17.
10 K. Akamatsu, T. Tsuruoka and H. Nawafune, *J. Am. Chem. Soc.*, 2005, **127**, 1634.
11 A. B. Djurisic, W. C. H. Choy, V. A. L. Roy, Y. H. Leung, C. Y. Kwong, K. W. Cheah, T. K. G. Rao, W. K. Chan, H. T. Lui and C. Surya, *Adv. Funct. Mater.*, 2004, **14**, 856.
12 J. R. Hahn and H. Kang, *Phys. Rev. B*, 1999, **60**, 6007.
13 X. Zhou, Q. Kuang, Z. Y. Jiang, Z. X. Xie, T. Xu, R. B. Huang and L. S. Zheng, *J. Phys. Chem. C*, 2007, **111**, 12091.
14 O. Diwald, M. Sterrer, E. Knozinger, P. V. Sushko and A. L. Shluger, *J. Chem. Phys.*, 2002, **116**, 1707.
15 R. Hacquart, J. M. Krafft, G. Costentin and J. Jupille, *Surf. Sci.*, 2005, **595**, 172.
16 M. L. Bailly, G. Costentin, H. Lauron-Pernot, J. M. Krafft and M. Che, *J. Phys. Chem. B*, 2005, **109**, 2404.
17 S. Stankic, M. Muller, O. Diwald, M. Sterrer, E. Knozinger and J. Bernardi, *Angew. Chem., Int. Ed.*, 2005, **44**, 4917.
18 A. Sternig, S. Stankic, M. Muller, J. Bernardi, E. Knozinger and O. Diwald, *Adv. Mater.*, 2008, **20**, 4840.
19 K. J. Klabunde and R. M. Richards, *Nanoscale Materials in Chemistry*, 2nd edn, Wiley-Interscience, 2009, pp. 21–26.
20 A. L. Shluger, P. V. Sushko and L. N. Kantorovich, *Phys. Rev. B*, 1999, **59**, 2417.
21 M. Muller, S. Stankic, O. Diwald, E. Knozinger, P. V. Sushko, P. E. Trevisanutto and A. L. Shluger, *J. Am. Chem. Soc.*, 2007, **129**, 12491.
22 C. Chizallet, G. Costentin, H. Lauron-Pernott, J. M. Krafft, M. Che, F. Delbecq and P. Sautet, *J. Phys.Chem. C*, 2008, **112**, 16629.
23 S. Stankic, M. Sterrer, P. Hofmann, J. Bernardi, O. Diwald and E. Knozinger, *Nano Lett.*, 2005, **5**, 1889.
24 M. Muller, A. Sternig, S. Stankic, M. Stoger-Pollach, J. Bernardi, E. Knozinger and O. Diwald, *J. Phys. Chem. C*, 2008, **112**, 9120.
25 A. Sternig, M. Muller, M. McCallum, J. Bernardi and O. Diwald, *Small*, 2010, **6**, 582.
26 H. R. Moon, J. J. Urban and D. J. Milliron, *Angew. Chem., Int. Ed.*, 2009, **48**, 6278.
27 J. V. Stark, D. G. Park, I. Lagadic and K. J. Klabunde, *Chem. Mater.*, 1996, **8**, 1904.
28 M. Chiesa, E. Giamello and M. Che, *Chem. Rev.*, 2010, **110**, 1320.
29 X. G. Han, M. S. Jin, Q. Kuang, Z. Z. X. Xie and L. S. Zheng, *J. Phys. Chem. C*, 2009, **113**, 2867.
30 X. G. Han, Y. Q. Jiang, S. F. Xie, Q. Kuang, X. Zhou, D. P. Cai, Z. X. Xie and L. S. Zheng, *J. Phys. Chem. C*, 2010, **114**, 10114.

